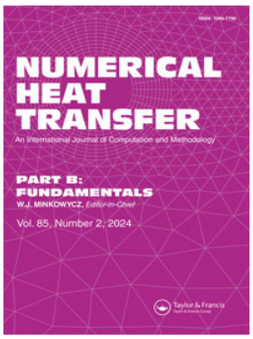

Taylor & Francis
Taylor & Francis Group

Numerical Heat Transfer, Part B: Fundamentals
An International Journal of Computation and Methodology

ISSN: (Print) (Online) Journal homepage: www.tandfonline.com/journals/unhb20

Chebyshev spectral approach to an exponentially space-based heat generating single-phase nanofluid flowing on an elongated sheet with angled magnetic field

MD. Shamshuddin, T. M. Agbaje, K. K. Asogwa, G. Makanda & Usman

To cite this article: MD. Shamshuddin, T. M. Agbaje, K. K. Asogwa, G. Makanda & Usman (2024) Chebyshev spectral approach to an exponentially space-based heat generating single-phase nanofluid flowing on an elongated sheet with angled magnetic field, Numerical Heat Transfer, Part B: Fundamentals, 85:2, 159-176, DOI: 10.1080/10407790.2023.2230355

To link to this article: https://doi.org/10.1080/10407790.2023.2230355

NUMERICAL HEAT TRANSFER, PART B: FUNDAMENTALS
2024, VOL. 85, NO. 2, 159–176
https://doi.org/10.1080/10407790.2023.2230355

Chebyshev spectral approach to an exponentially space-based heat generating single-phase nanofluid flowing on an elongated sheet with angled magnetic field

MD. Shamshuddin[a], T. M. Agbaje[b], K. K. Asogwa[c], G. Makanda[d], and Usman[e]

[a]Department of Compute Science and Artificial Intelligence, SR University, Warangal, Telangana, India; [b]School of Computer Science an Applied Mathematics, University of the Witwatersrand, Johannesburg, Private Bag 3, Braamfontein-2050, South Africa; [c]Department of Mathematics, Nigeria Maritime University, Okerenkoko, Delta State, Nigeria; [d]Department of Mathematical and Physical Sciences, Center for Sustainable Smart Cities, Central University of Technology, Braamfontein, South Africa; [e]Department of Computer Science, National University of Sciences and Technology, Balochistan Campus (NBC), Quetta, Pakistan

ABSTRACT

A novel mathematical model for radiative nanoliquid flow is developed as a result of stretching a sheet with an angled magnetic field that is submerged in nanoparticles. Joule dissipation and exponentially based heat source/sink effects is employed in the present phenomena under the heat constraints. The governing equations, which describe the flowing nanofluid are transformed into invariant dimensionless equations with suitable similarity quantities. With the adoption of a spectral quasi-linearization method, the resultant equations are numerically simplified. The impact of several converted dimensionless elements on physically interesting values is depicted visually. The current analysis is validated through comparison with some selected related literature, which shows a positive correlation. Inspired by applications, Advances in nanoscience and technology acquired the significance of the nanofluid in novel functional polymers like fiber insulation, geothermal system, and chemical catalytic reactors.

ARTICLE HISTORY
Received 8 February 2023
Revised 9 May 2023
Accepted 23 June 2023

KEYWORDS
Aqueous nanofluid; inertial drag; nanoparticles; thermal radiation; thermal slip

1. Introduction

A revolutionary heat transfer fluid termed as "nanofluid" has emerged because of scientific and nanotechnology advancements. Nanofluids are made up of nonmetallic or metallic nanometer sized particles (less than 100 nanometer) dispersed in various traditional fluids. There has been an explosion of study and invention utilizing amazing uses of nanofluids in industries including electrical cooling, solar energy, power generation, water heaters, biomedical, among others, over the previous few decades. The idea of nanofluids was suggested by Choi [1] at the NAL (National Argon Laboratory). The effective thermal conductivity of nanotube-in-oil suspensions is measured and proposes the usual thermal behavior which testifies the highest thermal conductivity [2]. The nanofluid is a suitable coolant and its excellent thermal properties contribute to the high heat transfer of the radiator. Arora and Gupta [3] investigated the hydrothermal performance of nanofluids in flat tube automobile radiators. Murshed and de Castro [4] evaluated the studies and improvement of conduction and convection warmth switch traits of ethylene glycol-primarily based totally nanofluids. The results demonstrated that those nanofluids own significantly better

CONTACT MD. Shamshuddin shammaths@gmail.com Department of Compute Science and Artificial Intelligence, SR University, Warangal-506371, Telangana, India.

thermal conductivity and convective warmth switch traits as compared to their base fluids that is ethylene glycol and its aqua mixture. Further relevant literature is found in Refs. [5–9].

The notion of Darcy flow is established upon the motion of fluids through a porous medium with small voids and spaces and low velocity. For the nonlinear velocity of the fluid, the concept of Darcy flows has transformed to the Darcy–Forchheimer model. Darcy–Forchheimer flows have numerous applications, for instance, drying of permeable materials in the textile industry, seepage of water in river beds, and the process of filtration and purification of water. Forchheimer [10] expanded the concept of Darcy by adding the square of velocity term in the momentum equation for calculation of inertial force and flow of boundary layer. Muskat [11] has identified the Forchheimer term. Sadiq and Hayat [12] have investigated Darcy–Forchheimer MHD fluid flow over a thermally heated surface. It has been concluded by the authors that the thermal relaxation parameter and Prandtl number are inversely related to the thermal characteristics of the flow system. Khan *et al.* [13] have investigated the irreversibility generation for fluid over a disk by considering the Darcy–Forchheimer nanofluid and have noticed that flow characteristics have decayed with augmentation in Forchheimer number and porosity parameter. Similar studies can be seen in Refs. [14–17].

In recent years, numerous scientists and researchers have been motivated to work on designing procedures where the impact of thermal radiation plays a critical role. It is acknowledged that the rate of heat transport is significantly regulated by the impact of thermal radiation. Therefore, numerous researchers have concentrated on studying and developing the heat transport mechanism in the presence of thermal radiation because the radiative heat transfer process plays vibrant part in all engineering and manufacturing processes, which includes furnace design, plasma physics, satellite and space vehicles, nuclear reactors, and designing pertinent equipment. Zhang *et al.* [18] studied heat transfer in nanofluids with magnetic strength and radiation through porous media analytically using differential transformation method. The effect of radiation on MHD nanofluid due to nonlinear shrinking/stretching plate is discussed by Pal and Mondal [19]. Das and Jana [20] discussed the impact of magnetized radiation on the convective nanoliquid along motioning sheet. They noticed high radiation declines fluid velocity and temperature distribution. Hayat *et al.* [21] considered radiative flow of Williamson liquid along a stretchy sheet with magnetic strength. Hayat *et al.* [22] examined thermal radiative MHD Maxwell fluid flow over stretched sheet. Shashikumar *et al.* [23] stated characteristics of magnetism with radiation on the flowing Casson liquid along permeable microchannel. Jha and Samalia [24] considered radiative effect on the fluid flowing in a flat plate boundary layer. Govindarajulu and Reddy [25] presented radiation impact on MHD pulsatile hybrid nanofluid flow. They concluded inclination in heat transfer rate for greater viscous dissipation and reverse behavior for higher magnetized radiation. Further recent applications developed in nanofluids are explored in Refs. [26–31].

The production of heat energy while using various tools and applications reduces a machine's efficiency. For the past few decades, scientists and engineers have been using conventional heat exchangers to solve such problems. Ethylene glycol, water, silicone oil, and other fluids are routinely utilized to minimize heat energy. Researchers and engineers have taken several different approaches to improve the thermal properties of these fluids due to their low efficiency. They discovered that adding solid particles to base fluid suspension could improve the ability of fluids to transmit heat. So, the production/generation of heat phenomenon is influenced much in the area of dynamics of fluids. Researchers in this direction are keenly interested. Geridonmez and Oztop [32] presented a numerical study of nanoparticles flow and heat transport in the duct under the influence of cross-differential magnetic fields. The findings were described by the isotherms, streamlines, vorticity contours and Nusselt number. The thermal conductivity increased due to an increase in the size of the heater or the distinct compositions of nanoparticles. Zhang and Zhang [33] probed the performance of pressure drop and heat transport of magnetic nanofluids with various varying magnetic fields. The outcomes revealed that varying magnetic fields have a

stronger effect on local thermal performance rather than nonmagnetic fields. Also, numerical simulations were performed by Zhang and Zhang [34] to study the thermal transmission and magnetic nanofluids flow properties under magnetic field intensities, magnetic field directions and volume fractions. Ramzan *et al.* [35] studied magnetic dipole effect for an Oldroyd-B fluid. According to their findings, the effect of the thermal performance was small in a poor magnetic field but increased significantly in a powerful magnetic field.

Keeping in view of aforesaid literature the current study is intended to carry out the behavior of thermophysical properties of silver and Gold nanoparticles on the water-based liquid over an inclined elongated sheet. The novelty of the study arises due to the Darcy–Forchheimer inertial drag on the flow through permeable medium. However, the exponential space-based heat source and thermal radiation also enriches the heat transport phenomenon. Spectral quasi-linearization method (SQLM) is deployed to solve the proposed designed model and the results are validate with the earlier investigation in particular cases.

2. Problem formulation analysis

Stretching flow of an incompressible water-based nanofluid consisting of Ag (silver) and Au (Gold) nanoparticles in an inclined magnetic field imposed elongated sheet of nanofluid boundary layer flow is considered in the current article. Thermal radiation, Joule heating, and exponentially space-based thermal generation are investigated in energy equation. The pure liquid and in thermal equilibrium solid volume nanoparticles were considered. The thermophysical attributes of the nanomaterial were shown in Table 1. Initially, the surface speed is due to $u = \lambda u_w(x)$, which specifies stretchy flow rate with a nonnegative constant λ through the horizontal axis x inclined with inclination γ. The stream is taken to be along x-axis and inclined magnetic field with strength B_0 is the introduced perpendicular magnetic field in the flow direction. At $\gamma = 90^o$ this magnetic field acts like a transverse magnetic field. At the sheet surface, the uniform temperature T_w, which is greater than the T_∞, denotes fluid ambient heat as depicted in Figure 1. In view of proposed assumptions, the developed equations from Refs. [36–38].

$$\frac{\partial u}{\partial x} + \frac{\partial v}{\partial y} = 0, \tag{1}$$

$$u\frac{\partial u}{\partial x} + v\frac{\partial u}{\partial y} = \frac{\mu_{nf}}{\rho_{nf}}\frac{\partial^2 u}{\partial y^2} - \frac{\mu_{nf}}{\rho_{nf}K_p^*}u - \frac{C_b}{\sqrt{K_p^*}}u^2 - \frac{\sigma_{nf}}{\rho_{nf}}B_0^2 u\ \sin^2\gamma, \tag{2}$$

$$\left.\begin{aligned} u\frac{\partial T}{\partial x} + v\frac{\partial T}{\partial y} = \left(\frac{k_{nf}}{(\rho c_p)_{nf}} + \frac{16\ \sigma^* T_\infty^3}{3k^*}\right)\frac{\partial^2 T}{\partial y^2} + \frac{\mu_{nf}}{(\rho c_p)_{nf}}\left(\frac{\partial u}{\partial y}\right)^2 + \frac{\sigma_{nf}}{(\rho c_p)_{nf}}B_0^2\ u^2\ \sin^2\gamma \\ + \frac{Q_e^{\bullet}}{(\rho c_p)_{nf}}e^{-\eta y\sqrt{\frac{a}{v_f}}}(T - T_\infty), \end{aligned}\right\} \tag{3}$$

Table 1. Following [41] thermodynamic properties of the nanoparticle with working fluid.

Thermodynamic terms	Working fluid H_2O (water)	Nanoparticles	
		Ag (Silver)	Au (Gold)
ρ (kg/m^3)	997.1	10500	19300
c_p (J/Kg K)	4179	235	129.1
k (W/mK)	0.613	401	318
σ (S/m)	0.05	6.3×10^7	4.52×10^7

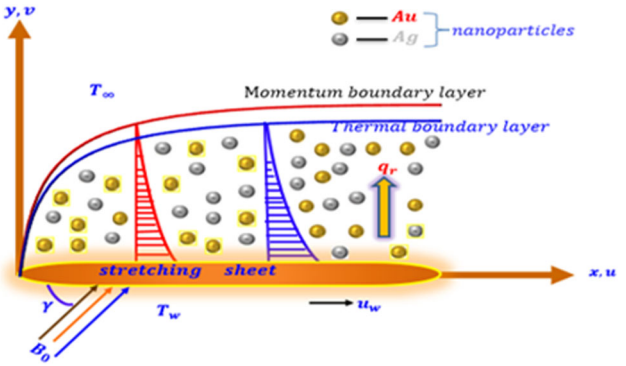

Figure 1. Geometry of the nanofluid flow for proposed problem.

The conditions at the boundary are [32, 39]

$$\left.\begin{aligned} u = \lambda u_w(x) + u^* \frac{\partial u}{\partial y}, \;\; v = 0, \;\; T = T_w + T^* \frac{\partial T}{\partial y}, \;\; at \;\; y = 0, \\ u \to 0, \;\; T \to T_\infty, \;\; as \;\; y \to \infty. \end{aligned}\right\} \tag{4}$$

Here, (u, v) denote velocity componenets. Dynamic viscosity of nanoliquid μ_{nf}, density ρ_{nf}, electrical conductivity σ_{nf}, thermal conductivity k_{nf}, specific heat $(\rho c_p)_{nf}$, magnetic field strength B_o, k_p^* is the dimenaional permeability term, c_b signifies Forchheimer resistance factor, $Q_e^{\bullet}$ is the dimensional exponentially space-based heat source/sink coefficient, σ^* is the Stefan Boltzmann number and k^* is the absorption coefficient

Now, for nanofluids, let us present the following expression for effective nanofluid properties followed by [40]

$$\left.\begin{aligned} \mu_{nf} = \mu_f \left[1 + 2.5\varphi + 4.5\left\{\frac{1}{\frac{h}{d_p}\left(2 + \frac{h}{d_p}\right)\left(1 + \frac{h}{d_p}\right)^2}\right\}\right], \;\; (\rho c_p)_{nf} = (\rho c_p)_f \left[(1-\varphi) + \varphi \frac{(\rho c_p)_s}{(\rho c_p)_f}\right], \\ (\rho)_{nf} = (\rho)_f \left[(1-\varphi) + \varphi \frac{(\rho)_s}{(\rho)_f}\right], \;\; (\sigma)_{nf} = (\sigma)_f \left[1 + \left(\frac{3\left(\frac{\sigma_s}{\sigma_f} - 1\right)\varphi}{\left(\frac{\sigma_s}{\sigma_f} + 2\right) - \left(\frac{\sigma_s}{\sigma_f} - 1\right)}\right)\right], \\ (k)_{nf} = (k)_f \left[\frac{k_s + 2k_f - 2\varphi(k_f - k_s)}{k_s + 2k_f + \varphi(k_f - k_s)}\right] \end{aligned}\right\} \tag{5}$$

The thermodynamic properties of the considered nanoparticle along with working fluid are tabulated following [41].

For the current model simplification, the defined subsequent similarity quantities are utilized

$$\eta = y\sqrt{\frac{a}{\nu_f}}, \;\; u = a\, x\, f', \;\; v = -\sqrt{a\, \nu_f}\, f, \;\; \theta = \frac{T - T_\infty}{T_w - T_\infty}. \tag{6}$$

The mutated momentum and heat mathematical equations associated with the boundary conditions expressed by Eqs. (2)–(6) may be stated as

$$\frac{A_1}{A_1} f''' - f'^2 + f\, f'' - \frac{A_1}{A_1} Da\, f' - Ir\, f'^2 - \frac{A_3}{A_2}\, M\, \sin^2\gamma\, f' = 0, \tag{7}$$

$$(A_4 + Rd)\theta'' + Pr\left\{f\theta' + \frac{A_1}{A_5}Ec\ f''^2 + \frac{A_3}{A_5}Ec\ M\ \sin^2\gamma\ f'^2 + \frac{1}{A_5}Q\ e^{-\eta n}\right\} = 0, \tag{8}$$

With the transformed boundary conditions,

$$\left.\begin{array}{ll} f(0) = 0,\ f'(0) = \lambda + \alpha\ f''(0),\ \theta(0) = 1 + \beta\ \theta'(0), & at\ \eta = 0, \\ f'(\infty) \to \infty,\ \theta(\infty) \to 0, & as\ \eta \to \infty. \end{array}\right\} \tag{9}$$

Where the primes refer to differentiation regard to similarity variable η and $M = \sigma_f B_0^2/a\rho_f$ gives a factor that indicates the magnetic parameter, $Da = \nu_f/aK_p^*$ is Porosity parameter, $Ir = x\ c_b/\sqrt{K_p^*}$ denotes local inertia, $Rd = 16\sigma^* T_\infty^3/3k^* k_f$ indicates the radiation factor, $Pr = \nu_f(\rho c_p)_f/k_f$ points out Prandtl number, $Ec = u_w^2/(c_p)_f\Delta T$ represents Eckert number, $Q = Q_e^{\bullet}/a(\rho c_p)_f$ stands for heat source/sink. Furthermore, the parameter arised in the boundary conditions are expressed as $\alpha = u^*\sqrt{a/\nu_f}$ momentum slip parameter, $\beta = T^*\sqrt{a/\nu_f}$ is thermal slip parameter and n denotes exponential index. Additionally, the nano-fluid constants arised in Eqs. (8)–(10) are respectively, are expressed as follows

$$A_1 = \frac{\mu_{nf}}{\mu_f},\ A_2 = \frac{\rho_{nf}}{\rho_f},\ A_3 = \frac{\sigma_{nf}}{\sigma_f},\ A_4 = \frac{k_{nf}}{k_f},\ A_5 = \frac{(\rho c_p)_{nf}}{(\rho c_p)_f} \tag{10}$$

2.1. Physical technological quantities of curiosity

To expression for skin friction factor and thermal transmission charecteristics of the model of current fluid movement, the quantities of physical important were pointed as skin friction factor and heat trnasmission factor expressed as

$$Cf_x = \frac{\tau_w}{\rho_f u_w^2},\ Nu_x = \left.\frac{xq_w}{k_f(T_w - T_\infty)}\right|_{y=0} \tag{11}$$

The dimensional thermal flux and solutal flux take the form:

$$\tau_w = \mu_{nf}\ \left.\frac{\partial u}{\partial y}\right|_{y=0},\ q_w = -\left.\left\{k_{nf}\ \frac{\partial T}{\partial y} + \frac{16\sigma^*}{3k^*}\frac{\partial T^4}{\partial y}\right\}\right|_{y=0} \tag{12}$$

Invoking the nondimensional transformations, we get

$$\left.\begin{array}{l} \sqrt{Re_x}\ Cf_x = A_1\ f''(0), \\ \dfrac{Nu_x}{\sqrt{Re_x}} = -(A_4 + Rd)\theta'(0) \end{array}\right\} \tag{13}$$

3. Methodology

In this part, the ordinary differential equations (ODEs) described in Eqs. (7) through (8) are numerically solved *via* the SQLM. To linearize the governing nonlinear equations, the SQLM is a numerical approach that utilizes the Newton–Raphson predicated on quasi-linearisation method (QLM), which was originally conceived by Bellman and Kalaba [42]. Using the Chebyshev spectral technique (CSA), integrate the linearized equations. The QLM system utilizes the Taylor series transformation to linearize nonlinear (ODEs) or partial differential equations under the implication that the disparity between the significance of the arbitrary function at the current iteration threshold signified by $s+1$ and the value at the previous iteration stage s is small. For a

thorough explanation of the procedure, read here (See Motsa [43]). Using the QLM on Eqs. (7) through (8) yields,

$$a_{0,s}\, f'''_{s+1} + a_{1,s} f''_{s+1} + \ a_{2,s} f'_{s+1} + \ a_{3,s} f_{s+1} = H_1, \tag{14}$$

$$b_{0,s}\theta''_{s+1} + \ b_{1,s}\theta'_{s+1} + \ b_{2,s} f''_{s+1} + \ b_{3,s} f'_{s+1} + \ b_{4,s} f_{s+1} = H_2, \tag{15}$$

where the variable coefficients $a_{i,s}$, and $b_{i,s}(i = 1, 2, 3, \ldots)$ derived from prior computations and characterized as:

$$\left.\begin{aligned} a_{0,s} = \frac{A_1}{A_2},\ a_{1,s} = f_s,\ a_{2,s} = -2f_s' - \frac{A_1}{A_2}Da + 2Irf_s' - \frac{A_3}{A_2}M\sin^2\gamma,\ a_{3,s} = f_s'', \\ b_{0,s} = A_4 + Rd,\quad b_{1,s} = Prf_s,\quad b_{2,s} = 2EcPr\frac{A_1}{A_5}f_s'', b_{3,s} = 2MEcPr\frac{A_3}{A_5}\sin^2\gamma f_s', \\ b_{4,s} = Pr\theta_s' \end{aligned}\right\} \tag{16}$$

The appropriate right part $H_i(1, 2, 3, \ldots)$ Eqs. (14) through (15) are outlined as follows:

$$\left.\begin{aligned} H_1 = a_{0,s} f'''_{s+1} + \ a_{1,s} f''_{s+1} + \ a_{2,r} f'_{s+1} + \ a_{3,s} f_{s+1} - R_1, \\ H_2 = b_{0,s}\theta''_{s+1} + \ b_{1,s}\theta'_{s+1} + \ b_{2,s} f''_{s+1} + \ b_{3,s} f'_{s+1} + \ b_{4,s} f_{s+1} - R_2, \end{aligned}\right\} \tag{17}$$

and $R_i(1, 2, 3, \ldots)$ are defined as:

$$\left.\begin{aligned} R_1 = \frac{A_1}{A_2}f'''_s - \ \left(f_s'\right)^2 + f_s f_s'' - \frac{A_3}{A_2}M\sin^2\gamma f_s' - \ \frac{A_1}{A_2}Daf_s' + Ir\ \left(f_s'\right)^2, \\ R_2 = (A_4 + Rd)\theta_s'' + Pr\left(f_s\theta_s' + \frac{A_1}{A_5}\ Ec\ \left(f_s''\right)^2 + \frac{A_3}{A_5}\ MEc\sin^2\gamma\left(f_s'\right)^2 + \frac{1}{A_5}Qe^{-n\eta}\right). \end{aligned}\right\} \tag{18}$$

The CSA is chosen to repeatedly solve Eqs. (14) and (15), beginning with a suitable initial guess provided as:

$$f_0(\eta) = \frac{\lambda}{1+\alpha} - \frac{\lambda}{1+\alpha}e^{-\eta},\ \ \theta_0(\eta) = \frac{1}{1+\beta}e^{-\eta}. \tag{19}$$

The starting guesses supplied in Eq. (19) are selected to satisfy the boundary-condition of (9).

Using the domain truncation technique, it is practical to convert the domain from $[0, \infty]$ to $[-1, 1]$. The subject is, therefore, addressed in the domain $[0, L]$ instead of $[0, \infty]$, where L is a positive integer sufficiently large to indicate the criterion at maximum. To transform the interval $[0, L]$ to $[-1, 1]$, the linear transformation $\eta = \frac{L(x+1)}{2}$, $\eta \in [0, \infty]$ and $x \in [-1, 1]$, is used. To approximate the derivatives of the not known variables $f(\eta)$, and $\theta(\eta)$, the differentiation matrix D is introduced at the collocation point.

The SQLM technique for Eqs. (14) and (15) is expressed in matrix notation as:

$$\begin{bmatrix} A_{11} & A_{12} \\ A_{21} & A_{22} \end{bmatrix}\begin{bmatrix} f_{s+1} \\ \theta_{s+1} \end{bmatrix} = \begin{bmatrix} H_1 \\ H_2 \end{bmatrix}, \tag{20}$$

where

$$\left.\begin{aligned} A_{11} = a_{0,s}\boldsymbol{D}^3 + diag[a_{1,s}]\boldsymbol{D}^2 + diag[a_{2,s}]D + diag[a_{3,s}], \\ A_{12} = 0, \\ A_{21} = diag[b_{2,s}]\boldsymbol{D}^2 + diag[b_{3,s}]D + diag[b_{4,s}], \\ A_{22} = b_{0,s}\boldsymbol{D}^2 + diag[b_{1,s}]D \end{aligned}\right\} \tag{21}$$

with diag indicate the diagonal matrix of size $(N_x + 1) \times (N_x + 1)$ and $\boldsymbol{D}$ signifies the differentiation with respect to η.

3.1. Results validation

In this study, the modeled equations were computed through spectral quasi-linearisation approach. To demonstrate the convergence of the SQLM numerical scheme, solution mistakes have been taken into account. The infinity norms are utilized to demonstrate the SQLM's convergence. The infinity norms are established by the following:

$$E_f = \max_{0\le j\le N_x} \|f_{s+1,j} - f_{s,j}\|_\infty,\ E_\theta = \max_{0\le j\le N_x} \|\theta_{s+1,j} - \theta_{s,j}\|_\infty\} \tag{22}$$

Again, we evaluate the SQLM's precision by calculating the residual error norm at infinity for each function. The infinity norm is calculated by substituting approximate solutions into differential Eqs. (7) and (8). The standards are described as:

$$\left.\begin{aligned} \|\mathrm{Res}\ (f)\|_\infty &= \left(\left\|\frac{A_1}{A_2}f'''_s - \left(f_s'\right)^2 + f_s f_s'' - \frac{A_3}{A_2}M\sin^2\gamma f_s' - \frac{A_1}{A_2}Daf_s' + Ir\ \left(f_s'\right)^2\right\|_\infty\right), \\ \|\mathrm{Res}\ (\theta)\|_\infty &= \left(\begin{array}{c} \|(A_4 + Rd)\theta_s'' + \\ Pr\left\{f_s\theta_s' + \frac{A_1}{A_5}\ Ec\ \left(f_s''\right)^2 + \frac{A_3}{A_5}\ M\ Ec\ \sin^2\gamma\left(f_s'\right)^2 + \frac{1}{A_5}Qe^{-n\eta}\right\}\|_\infty \end{array}\right) \end{aligned}\right\} \tag{23}$$

Table 2 illustrate the solution errors of E_f, and E_θ calculated with the SQLM at various repetition settings. As the number of iterations rises, the error norm in each of the functions decreases. This demonstrates that the SQLM numerical approach converges swiftly, as the error is detected to decline as the number of repetitions grows.

The residual error is depicted in Table 3 as a function of the number of repetitions. As the number of repetitions improves, the residual error diminishes, as seen in the table. The norm of the residual lowering indicates that the validity of the approximate solutions generated *via* SQLM improves as the number of iterations climbs. As the residual mean lowers, convergence is recognized to have occurred. The table's results imply that the SQLM is a reliable and accurate numerical method for solving nonlinear differential equations.

Table 4 presents the validation of computational results. The is demonstrate the accuracy of the adopted computational method and established the correctness of all presented results in this study through SQLM. As illustrated in Table 3, the SQLM outcomes show quantitative agreement with the existing computed outcomes (Gorla and Sidawi [44]; Khan and Pop [45]; Shah *et al.* [46]; and Hamad [40]). Which ensure us to impliment this new numerical algorithm in this article.

Table 2. Convergence of $f(\eta)$, and $\theta(\eta)$ obtained when $L = 30$, $N_x = 60$, $Q = 0.1$, $Pr = 6.2$, $n = 1$, $Rd = 1$, $M = 1$, $Ec = 0.5$, $\varphi = 0.3$, $n = 1$, $\alpha = 0.5$, $\beta = 0.5$, $Ir = 0.5$, $\lambda = 0.5$, and $\gamma = .\frac{\pi}{4}$

Iterations	E_f	E_θ
1	1.080×10^{-1}	4.274×10^{-1}
2	1.268×10^{-2}	1.199×10^{-2}
3	1.640×10^{-4}	5.432×10^{-3}
4	2.547×10^{-8}	3.374×10^{-6}
5	8.574×10^{-13}	3.017×10^{-13}
6	2.137×10^{-13}	3.897×10^{-13}
7	6.531×10^{-13}	6.128×10^{-13}
8	7.894×10^{-13}	9.099×10^{-13}
9	9.032×10^{-13}	1.454×10^{-13}
10	4.876×10^{-13}	5.208×10^{-13}

Table 3. Residual error for Eqs. (7) and (8) when $L = 30$, $N_x = 60$, $Q = 0.1$, $Pr = 6.2$, $n = 1$, $Rd = 1$, $M = 1$, $Ec = 0.5$, $\varphi = 0.3$, $n = 1$, $\alpha = 0.5$, $\beta = 0.5$, $Ir = 0.5$, $\lambda = 0.5$, and $\gamma = .\frac{\pi}{4}$

Iterations	$\|\text{Res } (f)\|_\infty$	$\|\text{Res } (\theta)\|_\infty$
1	2.074×10^{-3}	5.667×10^{-2}
2	1.703×10^{-5}	1.141×10^{-3}
3	2.073×10^{-9}	5.270×10^{-7}
4	3.476×10^{-13}	1.028×10^{-11}
5	3.216×10^{-13}	1.724×10^{-12}
6	1.436×10^{-13}	1.447×10^{-12}
7	1.667×10^{-13}	2.832×10^{-12}
8	3.496×10^{-13}	4.193×10^{-12}
9	2.404×10^{-13}	2.884×10^{-12}
10	3.141×10^{-13}	3.116×10^{-12}

Table 4. Comparison of $-\theta'(0)$, for different values of Pr when $A_1 = 1$, $A_2 = 1$, $A_3 = 1, A_4 = 1$, $A_5 = 1$, $Ir = 0$, $\beta = 0$, $Da = 0$, $M = 0$, $Ec = 0$, $Q = 0$, $Rd = 0$, $\lambda = 1$, and $\alpha = 0$.

Pr	Gorla and Sidawi [44]	Khan and Pop [45]	Shah *et al.* [46]	Hamad [40]	Present
0.07	0.06562	0.0663	0.06562258312843	0.06556	0.06562
0.2	0.16562	0.1691	0.169088618141040	0.16909	0.16912
0.7	0.53488	0.4539	0.453916816202306	0.45391	0.53488
2.0	0.91142	0.9113	0.911361392450143	0.91136	0.91142
3.0	1.15970	–	–	–	1.15970
7.0	1.89046	1.8954	1.895420199527724	1.89540	1.89046
10.0	2.30350	–	–	–	2.30350
20.0	3.35391	3.3539	3.353934997970873	3.35390	3.35391
50.0	5.42474	–	–	–	5.42474
70.0	6.46221	6.4621	6.462312632472948	6.46220	6.46221

Table 5. Numerical values of $\sqrt{Re_x}\ Cf_x$ for different values of φ, M, Da, Ir, λ, and α obtained when $L = 30$, $N_x = 60$, $Pr = 6.2$, $Ec = 0.5$, $Rd = 1$, $Q = 0.1$, $n = 1$, $\gamma = \frac{\pi}{4}$, and $\beta = 0.5$.

φ	M	Da	Ir	λ	α	$\sqrt{Re_x}\ Cf_x$
0	1	0.5	0.5	0.5	0.5	−0.35541
0.1						−0.37272
0.2						−0.38747
0.3						−0.40031
0.3	0	0.5	0.5	0.5	0.5	−0.36594
	0.5					−0.38410
	1.0					−0.40031
	1.5					−0.41493
0.3	1	0.01	0.5	0.5	0.5	−0.36671
		0.10				−0.37346
		1				−0.42821
		2				−0.47153
0.3	1	0.5	0	0.5	0.5	−0.42113
			1			−0.37418
			1.5			−0.33927
			2			−0.28711
0.3	1	0.5	0.5	0.1	0.5	−0.07016
				0.2		−0.14626
				0.3		−0.22715
				0.4		−0.31203
0.3	1	0.5	0.5	0.5	0	−0.75997
					0.2	−0.55315
					0.4	−0.44012
					0.6	−0.36750

4. Results and discussion of graphical interpretation

To find the numerical (SQLM) solution of transmutted ordinary differential Eqs. (7)–(9) for the (Ag/Au) nanofluid flow in a Darcy–Forchhmeir porous media upon a stretching surface with various novel effects. During the process, many parameters have emerged, which are discussed in

Table 6. Numerical values of $\frac{Nu_x}{\sqrt{Re_x}}$ for different values of φ, M, Rd, Ec, n, and β obtained when $L = 30$, $N_x = 60$, $Pr = 6.2$, $Ir = 0.5$, $Da = 0.5$, $Q = 0.1$, $\alpha = 0.5$, $\gamma = \frac{\pi}{4}$, and $\lambda = 0.5$.

φ	M	Rd	Ec	n	β	Q	$\frac{Nu_x}{\sqrt{Re_x}}$
0	1	1	0.5	1	0.5	0.1	0.321940
0.1							0.60472
0.2							0.73334
0.3							0.82738
0.3	0	1	0.5	1	0.5	0.1	0.97395
	0.5						0.89608
	1.0						0.82738
	1.5						0.76650
0.3	1	0	0.5	1	0.5	0.5	0.78079
		0.5					0.80588
		2					0.86272
		4					0.91653
0.3	1	1	0	1	0.5	0.1	0.88105
			0.05				0.87569
			1.0				0.77370
			3				0.55899
0.3	1	1	0.5	1	0.5	0.1	0.82738
				2			0.89141
				3			0.91328
				4			0.92439
0.3	1	1	0.5	1	0	0.1	0.92132
					0.5		0.82738
					1		0.75082
					1.5		0.68723
0.3	1	1	0.5	1	0.5	−0.4	1.48549
						−0.2	1.2225
						0	0.95900
						0.4	0.43251

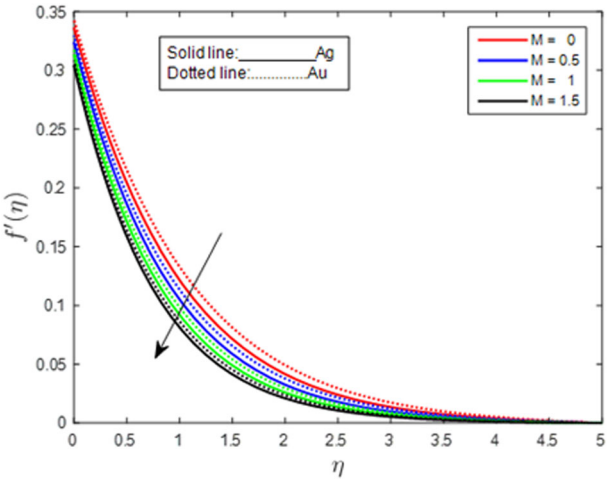

Figure 2. Effect of M on $f'(\eta)$ $L = 30$, $N_x = 60$, $Q = 0.1$, $Pr = 6.2$, $n = 1$, $Rd = 1$, $Ec = 0.5$, $\varphi = 0.3$, $n = 1$, $Ir = 0.5$, $\alpha = 0.5$, $\beta = 0.5$, $\lambda = 0.5$, and $\gamma = \frac{\pi}{4}$.

detail. The effects of various dimension-free parameters are measured for various types of nanoparticles, which are Ag (silver) and Au (gold) with water as base fluid.

Figures 2–16 and Tables 5 and 6 discuss the physical chareacteristics of flow in terms of $f'(\eta)$ (velocity), $\theta(\eta)$ (temperature) profiles, skin friction, and Nusselt number coefficients as well as to explain the physical interpretations induced by the dominant dimensionless components.

The impact of the magnetic field parameter (M) on $f'(\eta)$ for (Ag) silver nanofluid and (Au) gold nanofluid is shown in Figure 2. Comparatively, for both gold and silver nanofluids with an enhanced

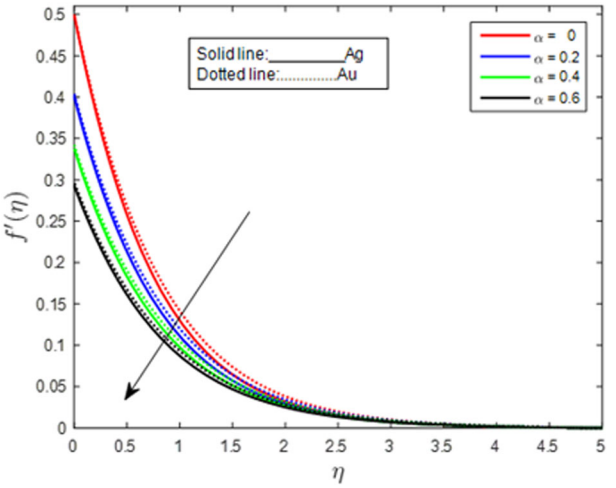

Figure 3. Effect of α on $f'(\eta)$ $L = 30$, $N_x = 60$, $Q = 0.1$, $Pr = 6.2$, $n = 1$, $Rd = 1$, $Ec = 0.5$, $\varphi = 0.3$, $n = 1$, $M = 1$, $\beta = 0.5$, $Ir = 0.5$, $\lambda = 0.5$, and $\gamma = \frac{\pi}{4}$.

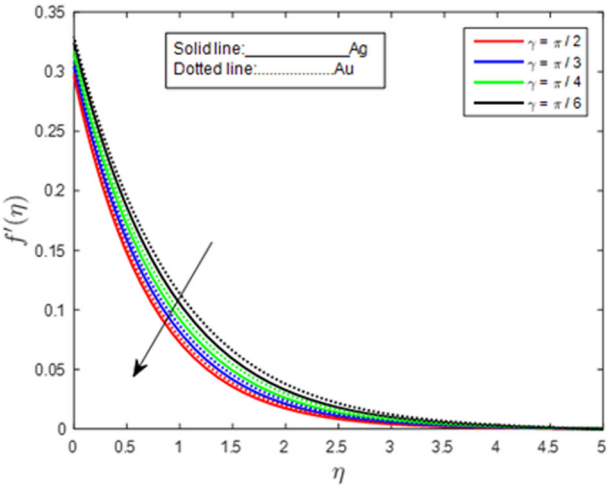

Figure 4. Effect of γ on $f'(\eta)$ $L = 30$, $N_x = 60$, $Q = 0.1$, $Pr = 6.2$, $n = 1$, $Rd = 1$, $Ec = 0.5$, $\varphi = 0.3$, $n = 1$, $M = 1$, $\beta = 0.5$, $Ir = 0.5$, and $\lambda = 0.5$.

magnetic parameter, the velocity distribution depletes. In comparison to gold nanoparticles, silver nanoparticles deteriorate more quickly. Physically, the magnetic field parameter creates the Lorentz force, which reduces the fluid's nanoparticles' downward motion velocity. Figure 3 demonstrates the influence of momentum slip parameter $(\alpha = 0, 0.2, 0.4, 0.6)$ on $f'(\eta)$ for silver nanofluid and gold nanofluid. With the thermal effect, less speed is achieved at the momentum boundary layer for both cases of nanoparticles as the momentum slip parameter rises with a dispersed effect.

The effect of the angle of inclination (γ) on $f'(\eta)$ de-escalate for water conveying silver and gold nanoparticles are displayed in Figure 4. Due to heat diffusion, the angle of inclination seems to lessen the magnetic field's impact. As a result, the fluid's driving magnetic field loses some of its strength, and its velocity ultimately decreases. Figure 5 shows the implication of the local inertia parameter (Ir) on $f'(\eta)$ for combined gold and silver nanofluids. The growing values of the local inertia parameter (Ir) accelerate the fluid velocity for both nanoparticles. Physically, the several atomic structures of the nanofluid under consideration uplift the migration of nanoparticles, improving the mobility of nanofluid despite the fluid resistance. Consequently, the velocity distribution of (Ag) silver nanofluid and (Au) gold nanofluid augment rapidly.

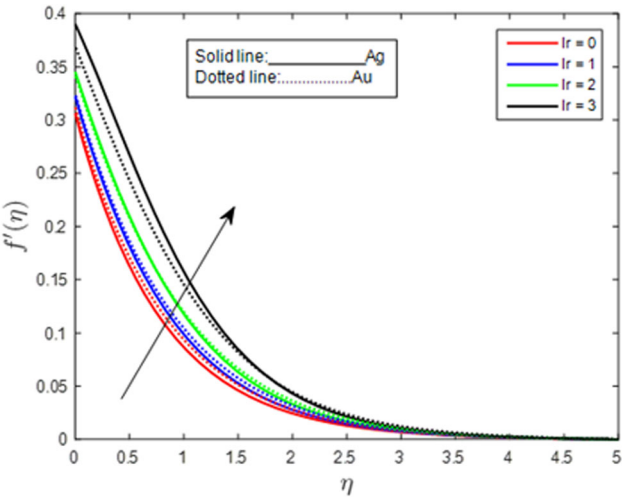

Figure 5. Effect of α on $f'(\eta)$ $L = 30$, $N_x = 60$, $Q = 0.1$, $Pr = 6.2$, $n = 1$, $Rd = 1$, $Ec = 0.5$, $Ir = 0.5$, $\varphi = 0.3$, $n = 1$, $M = 1$, $\beta = 0.5$, $\lambda = 0.5$, and $\gamma = \frac{\pi}{4}$.

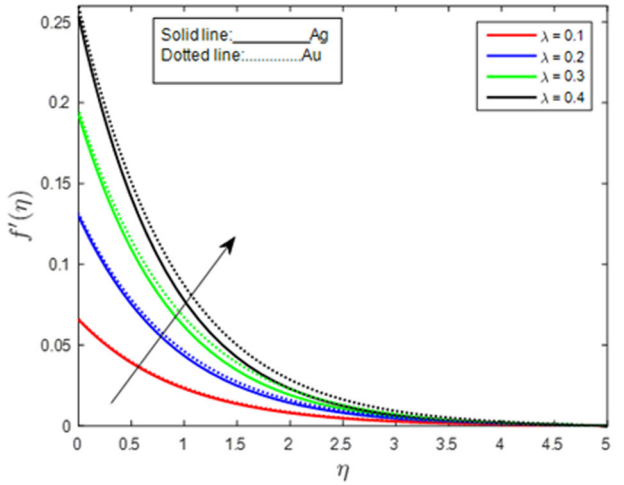

Figure 6. Effect of λ on $f'(\eta)$ $L = 30$, $N_x = 60$, $Q = 0.1$, $Pr = 6.2$, $n = 1$, $Rd = 1$, $Ec = 0.5$, $\varphi = 0.3$, $n = 1$, $M = 1$, $\beta = 0.5$, $\alpha = 0.5$, $Ir = 0.5$, and $\gamma = \frac{\pi}{4}$.

Figure 6 illustrates the pattern of $f'(\eta)$ for silver and gold nanofluids with increasing stretching constant (λ). As the fluid thermal efficiency is increased, the mean movements of the silver and gold nanofluids are boosted, resulting in an expanding velocity field as the values of the stretching constant progress. The impact of silver and gold nanoparticle volume fraction (ϕ) on $f'(\eta)$ distribution is shown in Figure 7. The thermal conductivity of silver nanofluid is demonstrated to be higher than that of gold nanofluid. The reason for this is that silver has a stronger thermal coefficient and heat capacity than gold nanoparticles. As a measure, the velocity distribution is subdued, increasing the rate at which the nanostructures with thermal diffusion. The effect of the thermal slip parameter (β) on $\theta(\eta)$ for (Ag) silver nanofluid and (Au) gold nanofluid is demonstrated in Figure 8. A boost in the thermal slip parameter of the system's thermal diffusion inhibits the heat content in the nanofluid flow environment, resulting in a decrease in the nanoparticle interface. Consequently, increasing thermal slip parameter values depletes the temperature distribution along the flow pattern.

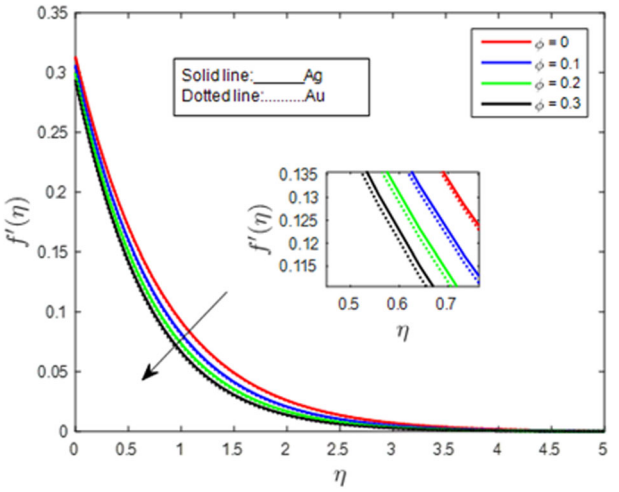

Figure 7. Effect of φ on $f'(\eta)$ when $L = 30$, $N_x = 60$, $Q = 0.1$, $Pr = 6.2$, $n = 1$, $Rd = 1$, $Ec = 0.5$, $Ir = 0.5$, $\alpha = 0.5$, $n = 1$, $M = 1$, $\beta = 0.5$, $\lambda = 0.5$, and $\gamma = \frac{\pi}{4}$.

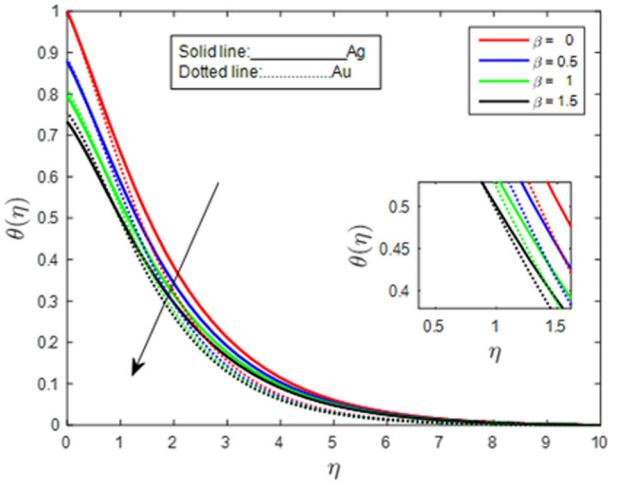

Figure 8. Effect of β on $\theta(\eta)$ when $L = 30$, $N_x = 60$, $Q = 0.1$, $Pr = 6.2$, $n = 1$, $Rd = 1$, $Ec = 0.5$, $Ir = 0.5$, $\alpha = 0.5$, $n = 1$, $M = 1$, $\varphi = 0.3$, $\lambda = 0.5$, and $\gamma = \frac{\pi}{4}$.

Figure 9 shows the effect of the Eckert number (Ec) on $\theta(\eta)$ for (Ag) silver nanofluid and (Au) gold nanofluids. The Eckert number depicts the connection between the kinetic energy of the flow and the enthalpy. It incorporates the transformation of kinetic energy into internal energy through the work performed against viscous fluid forces. The positive Eckert number indicates sheet cooling. Consequently, increased viscous dissipative heat causes a temperature increase in the nanofluids. The angle of inclination (γ) on $\theta(\eta)$ accelerates the nanofluids as displayed in Figure 10. Moreso, the influence of magnetic parameter on $\theta(\eta)$ as depicted in Figure 11 boost the temperature distribution of the nanofluids. Physically, thermal conductivity improves as the magnetic parameter increases; hence, the temperature rises.

In Figure 12, nonetheless, a large reduction in the temperature distribution is noted as the exponential index (n) approaches its maximum value. The effect of the nanoparticle volume fraction (ϕ) on $\theta(\eta)$ for (Ag) silver nanofluid and (Au) gold nanofluid is demonstrated in Figure 13. The volume percentage of nanoparticles increases as heat transmission increases. Since this demonstrates the actual influence of nanoparticles scattered in a liquid-based fluid boosting the thermal conductivities of silver and gold nanofluids.

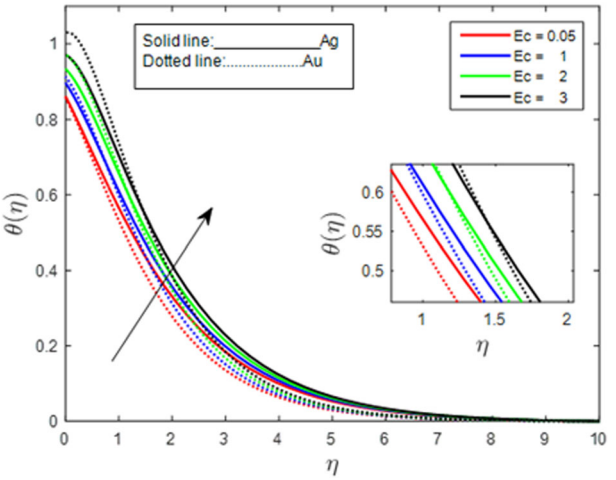

Figure 9. Effect of *Ec* on $\theta(\eta)$ when $L = 30,\ N_x = 60,\ Q = 0.1,\ Pr = 6.2,\ n = 1,\ Rd = 1,\ \varphi = 0.3,\ Ir = 0.5,\ \alpha = 0.5,\ M = 1,\ \beta = 0.5,\ \lambda = 0.5,$ and $\gamma = \frac{\pi}{4}$.

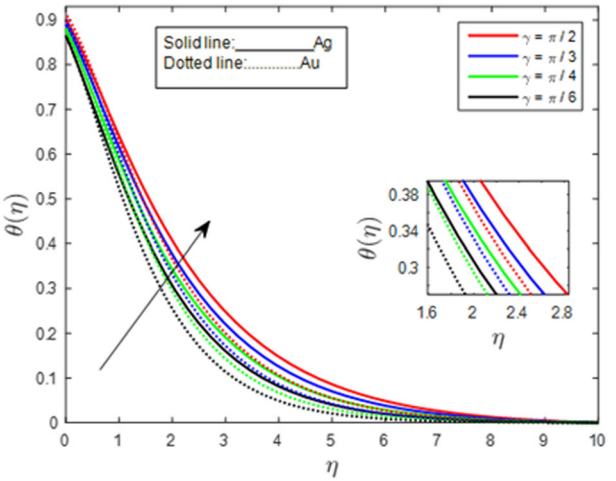

Figure 10. Effect of γ on $\theta(\eta)$ when $L = 30,\ N_x = 60,\ Q = 0.1,\ Pr = 6.2,\ Rd = 1,\ Ec = 0.5,\ Ir = 0.5,\ \alpha = 0.5,\ n = 1,\ M = 1,\ \beta = 0.5,\ \lambda = 0.5,$ and $\varphi = 0.3$.

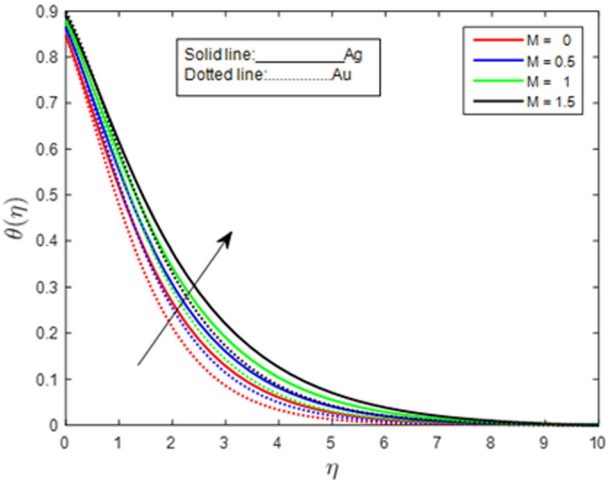

Figure 11. Effect of *M* on $\theta(\eta)$ when $L = 30,\ N_x = 60,\ Q = 0.1,\ Pr = 6.2,\ n = 1,\ Rd = 1,\ Ir = 0.5,\ Ec = 0.5,\ \alpha = 0.5,\ \varphi = 0.3,\ \beta = 0.5,\ \lambda = 0.5,$ and $\gamma = \frac{\pi}{4}$.

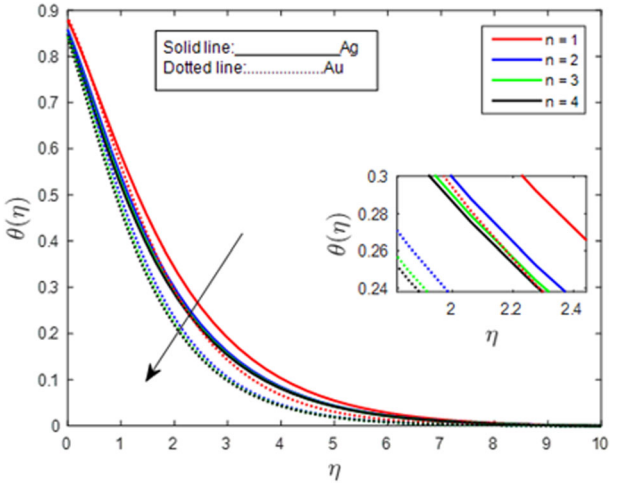

Figure 12. Effect of n on $\theta(\eta)$ when $L = 30$, $N_x = 60$, $Q = 0.1$, $Pr = 6.2$, $n = 1$, $Rd = 1$, $Ir = 0.5$, $Ec = 0.5$, $\alpha = 0.5$, $\varphi = 0.3$, $M = 1$, $\beta = 0.5$, $\lambda = 0.5$, and $\gamma = \frac{\pi}{4}$.

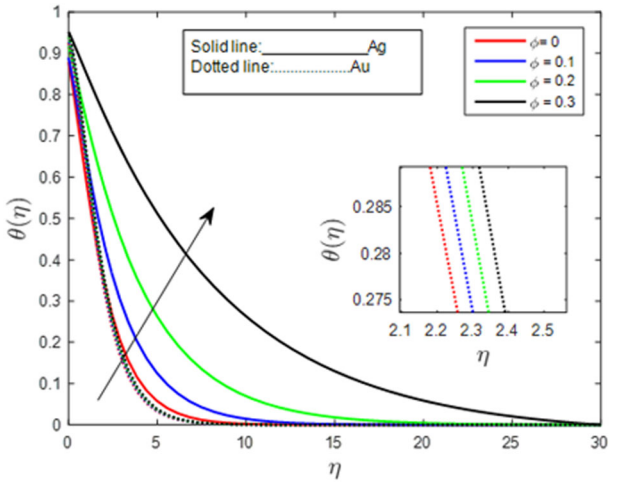

Figure 13. Effect of φ on $\theta(\eta)$ when $L = 30$, $N_x = 60$, $Q = 0.1$, $Pr = 6.2$, $n = 1$, $Rd = 1$, $Ir = 0.5$, $Ec = 0.5$, $\alpha = 0.5$, $n = 1$, $M = 1$, $\beta = 0.5$, $\lambda = 0.5$, and $\gamma = \frac{\pi}{4}$.

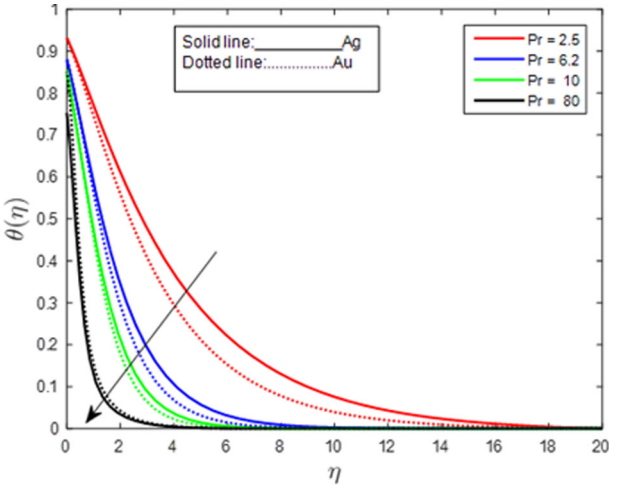

Figure 14. Effect of Pr on $\theta(\eta)$ when $L = 30$, $N_x = 60$, $Q = 0.1$, $\varphi = 0.3$, $n = 1$, $Rd = 1$, $Ir = 0.5$, $Ec = 0.5$, $\alpha = 0.5$, $n = 1$, $M = 1$, $\beta = 0.5$, $\lambda = 0.5$, and $\gamma = \frac{\pi}{4}$.

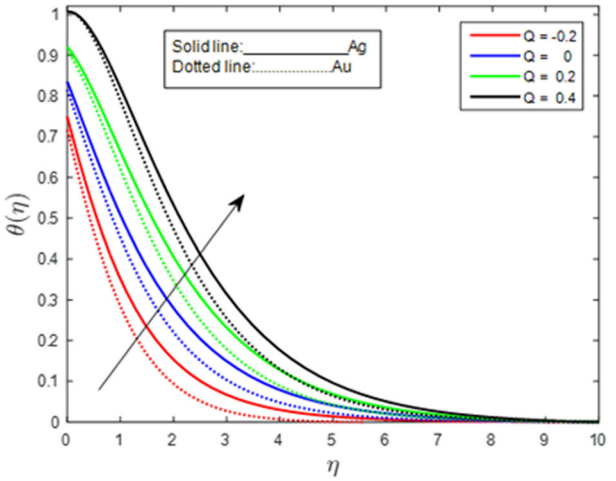

Figure 15. Effect of Q on $\theta(\eta)$ when $L = 30$, $N_x = 60$, $\varphi = 0.3$, $Pr = 6.2$, $n = 1$, $Rd = 1$, $Ir = 0.5$, $Ec = 0.5$, $\alpha = 0.5$, $n = 1$, $M = 1$, $\beta = 0.5$, $\lambda = 0.5$, and $\gamma = \frac{\pi}{4}$.

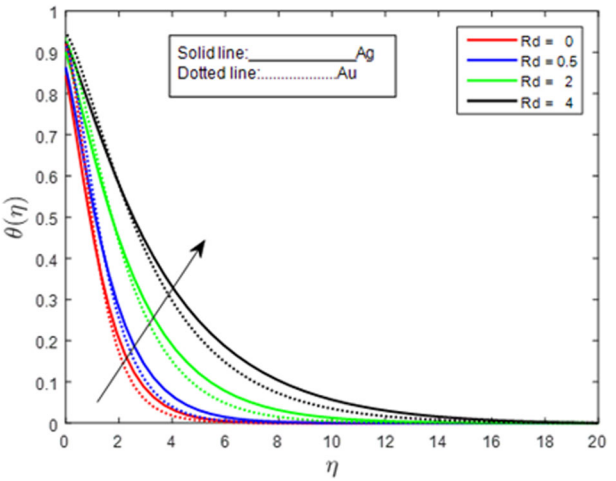

Figure 16. Effect of Rd on $\theta(\eta)$ when $L = 30$, $N_x = 60$, $Q = 0.1$, $Pr = 6.2$, $n = 1$, $\varphi = 0.3$, $Ir = 0.5$, $Ec = 0.5$, $\alpha = 0.5$, $n = 1$, $M = 1$, $\beta = 0.5$, $\lambda = 0.5$, and $\gamma = \frac{\pi}{4}$.

Figure 14 portrays the effect of the Prandtl number (Pr) on $\theta(\eta)$ for (Ag) silver nanofluid and (Au) gold nanofluid. The Prandtl number is the ratio of momentum diffusion to thermal diffusion and theory impact on temperature field are examined for different nanoparticles considered. It is recognized that the temperature of nanofluids decreases as the Prandtl number rises. Where gold nanoparticles exhibit a starting larger decrease than silver nanoparticles on the thermal boundary layer thickness for the temperature field as the Prandtl number increases. Since nanofluids have greater thermal conductivities as a result of a decrease in Prandtl numeric values, Asogwa *et al.* [47, 48].

It is shown in Figures 15 and 16 that uplifting heat source/sink and radiation parameters on $\theta(\eta)$ for (Ag) silver nanofluid and (Au) gold nanofluid boost temperature distribution as expected. Comparatively, it is observed that for both nanofluids that silver nanofluid shows a higher impact over gold nanofluid due to the stronger thermal conductivity of silver nanoparticles.

The measured numerical approximation for the coefficients of skin friction $\left(\sqrt{Re_x}C_f\right)$ and Nusselt number $Nu_x/\sqrt{Re_x}$ are presented in Tables 5 and 6, respectively, for the nanofluids. For

silver and gold nanofluids, it is obvious from Table 5 that the $\left(\sqrt{Re_x}C_f\right)$ amplifies as local inertia and momentum slip parameters become stronger with a rapid reduction considering nanoparticle volume fraction, magnetic parameter and porosity parameter. In Table 6, the $Nu_x/\sqrt{Re_x}$ depletes by growing values of Eckert number, magnetic field, thermal slip, and heat source/sink parameters while heat transmission is noticed for progressive values of nanoparticle volume fraction, radiation parameter, and exponential index.

5. Conclusion

This article develops a numerically reduced model with the application of the spectral quasi-linearization technique to the associated equations for the flow of MHD nanofluids across an elongated sheet. Consideration is given to the scattering of silver and gold nanoparticles in water as a base fluid in the presence of heat generation and absorption. The impact of the thermophysical attributes is quantified and reported for the velocity flow and temperature distribution in graphs and tables. As a result of the investigation, the following are the important conclusions of this examination:

- The velocity distribution of nanofluids depletes with the upsurge of magnetic parameter, momentum slip parameter, and angle of inclination with a significant decline of silver nanoparticles over gold nanoparticles.
- The local inertia escalates the momentum distribution of the nanofluids with silver nanofluid having a greater effect over gold nanofluid.
- The heat source, radiation, magnetic, viscous dissipative parameters, and nanoparticles boost temperature distribution while thermal slip, exponential index, and Prandtl number degrade thermal profiles for the nanofluids.
- The thermal transfer decreases as the Eckert number, magnetic field, thermal slip, and heat source/sink parameters increase, while heat transmission increases as the nanoparticle volume percentage, radiation parameter, and exponential index increase for the nanofluids.

ORCID

MD. Shamshuddin http://orcid.org/0000-0002-2453-8492
K. K. Asogwa http://orcid.org/0000-0002-5623-0492

References

[1] S. U. S. Choi, "Enhancing thermal conductivity of fluids with nanoparticles," in *Developments and Applications of Non-Newtonian Flows*, vol. 66, D. A. Siginer and H. P. Wang, Eds. New York: American Society of Mechanical Engineers, 1995, pp. 99–105.

[2] S. U. S. Choi, Z. G. Zhang, W. Yu, F. E. Lockwood, and E. A. Grulke, "Anomalous thermal conductivity enhancement in nanotube suspensions," *Appl. Phys. Lett.*, vol. 79, no. 14, pp. 2252–2254, 2001. DOI: 10.1063/1.1408272.

[3] N. Arora and M. Gupta, "An updated review on application of nanofluids in flat tubes radiators for improving cooling performance," *Renew. Sust. Energy Rev.*, vol. 134, pp. 110242, 2020. DOI: 10.1016/j.rser.2020.110242.

[4] S. S. Murshed and C. N. de Castro, "Conduction and convection heat transfer characteristics of ethylene glycol based nanofluids–A review," *Appl. Energy*, vol. 184, pp. 681–695, 2016. DOI: 10.1016/j.apenergy.2016.11.017.

[5] K. V. Wong and O. De Leon, "Applications of nanofluids: Current and future," in *Nanotechnology Energy*. New York: Jenny Stanford Publishing, 2017, pp. 105–132.

[6] K. Khanafer and K. Vafai, "A review on the applications of nanofluids in solar energy field," *Renew. Energy*, vol. 123, pp. 398–406, 2018. DOI: 10.1016/j.renene.2018.01.097.

[7] M. R. Safaei *et al.*, "Thermal analysis of a binary base fluid in pool boiling system of glycol–water alumina nano-suspension," *J. Therm. Anal. Calorim.*, vol. 143, no. 3, pp. 2453–2462, 2021. DOI: 10.1007/s10973-020-09911-5.

[8] MD. Shamshuddin, F. Mabood, W. A. Khan, and G. R. Rajput, "Exploration of thermal Peclet number, Vortex viscosity and Reynolds number on two-dimensional flow of micropolar fluid through a channel due to mixed convection," *Heat Transf.*, vol. 52, no. 1, pp. 854–873, 2023. DOI: 10.1022/htj.22719.

[9] T. K. Kumar and MD. Shamshuddin, "Thermal performance on radiative and Ohmic dissipative magneto-nanoliquid over moving flat plate suspended by SWCNTs and MWCNTs," *J. Nanofluids*, vol. 12, no. 1, pp. 192–201, 2023. DOI: 10.1166/jon.2023.1945.

[10] P. Forchheimer, *Wasserbewegung Durch Boden*, 45th ed. Z. Ver. Deutsch, Ing., 1901.

[11] M. Muskat, *The Flow of Homogeneous Fluids through Porous Media*. New York, NY: McGraw-Hill Book Company, 1937.

[12] M. A. Sadiq and T. Hayat, "Darcy–Forchheimer flow of magneto Maxwell liquid bounded by convectively heated sheet," *Res. Phys.*, vol. 6, pp. 884–890, 2016. DOI: 10.1016/j.rinp.2016.10.019.

[13] M. I. Khan, F. Alzahrani, A. Hobiny, and Z. Ali, "Fully developed second order velocity slip Darcy-Forchheimer flow by a variable thicked surface of disk with entropy generation," *Int. Commun. Heat Mass Transf.*, vol. 117, pp. 104778, 2020. DOI: 10.1016/j.icheatmasstransfer.2020.104778.

[14] G. Rasool, A. Shafiq, and D. Baleanu, "Consequences of Soret-Dufour effects, thermal radiation, and binary chemical reaction on Darcy Forchheimer flow of nanofluids," *Symmetry*, vol. 12, no. 9, pp. 1421, 2020. DOI: 10.3390/sym12091421.

[15] A. A. Khan, S. Naeem, R. Ellahi, S. M. Sait, and K. Vafai, "Dufour and Soret effects on Darcy–Forchheimer flow of second-grade fluid with the variable magnetic field and thermal conductivity," *HFF*, vol. 30, no. 9, pp. 4331–4347, 2020. DOI: 10.1108/HFF-11-2019-0837.

[16] MD. Shamshuddin *et al.*, "MHD bioconvection microorganism nanofluid driven by a stretchable plate thorugh porous media with an induced heat source," *Waves Random Complex Media*, 2022. DOI: 10.1080/17455030.2022.2126024.

[17] MD. Shamshuddin *et al.*, "Thermo-solutal stratification and chemical reaction effects on radiative magnetized nanofluid flow along an exponentially stretching sensor plate: Computational analysis," *J. Magn. Magn. Mat.*, vol. 565, pp. 170286, 2023. DOI: 10.1016/j.jmmm.2022.170286.

[18] C. Zhang, L. Zheng, X. Zhang, and G. Chen, "MHD flow and radiation heat transfer of nanofluids in porous media with variable surface heat flux and chemical reaction," *Appl. Math. Model.*, vol. 39, no. 1, pp. 165–181, 2015. DOI: 10.1016/j.apm.2014.05.023.

[19] D. Pal and G. Mandal, "Hydromagnetic convective–radiative boundary layer flow of nanofluids induced by a non-linear vertical stretching/shrinking sheet with viscous–Ohmic dissipation," *Pow. Technol.*, vol. 279, pp. 61–74, 2015. DOI: 10.1016/j.powtec.2015.03.043.

[20] S. Das and R. N. Jana, "Natural convective magneto-nanofluid flow and radiative heat transfer past a moving vertical plate," *Alex. Eng. J.*, vol. 54, no. 1, pp. 55–64, 2015. DOI: 10.1016/j.aej.2015.01.001.

[21] T. Hayat, A. Shafiq, and A. Alsaedi, "Hydromagnetic boundary layer flow of Williamson fluid in the presence of thermal radiation and Ohmic dissipation," *Alex. Eng. J.*, vol. 55, no. 3, pp. 2229–2240, 2016. DOI: 10.1016/j.aej.2016.06.004.

[22] T. Hayat, S. Qayyum, S. A. Shehzad, and A. Alsaedi, "Simultaneous effects of heat generation-absorption and thermal radiation in magnetohydrodynamics (MHD) flow of Maxwell nanofluid towards a stretched surface," *Res. Phys.*, vol. 7, pp. 562–573, 2017. DOI: 10.1016/j.rinp.2016.12.009.

[23] N. S. Shashikumar, B. C. Prasannakumara, B. J. Gireesha, and O. D. Makinde, "Thermodynamics analysis of MHD Casson fluid slip flow in a porous microchannel with thermal radiation," *DF.*, vol. 16, pp. 120–139, 2018. DOI: 10.4028/www.scientific.net/DF.16.120.

[24] B. K. Jha and G. Samaila, "Thermal radiation effect on boundary layer over a flat plate having convective surface boundary condition," *SN Appl. Sci.*, vol. 2, no. 3, pp. 1–8, 2020. DOI: 10.1007/s42452-020-2167-8.

[25] K. Govindarajulu and A. S. Reddy, "Magnetohydrodynamic pulsatile flow of third grade hybrid nanofluid in a porous channel with Ohmic heating and thermal radiation effects," *Phys. Fluids*, vol. 34, no. 1, pp. 013105, 2022. DOI: 10.1063/5.0074894.

[26] M. Ramzan, N. Shahmir, H. A. S. Ghazwani, and M. Y. Malik, "Comparative appraisal of nanofluid flows in a vertical channel with constant wall temperatures: An application to the rocket engine nozzle," *Waves Random Complex Media*, 2022. DOI: 10.1080/17455030.2022.2102695.

[27] M. Ramzan, N. Shahmir, and H. A. S. Ghazwani, "Hybrid nanofluid flow comprising spherical shaped particles with Hall current and irreversibility analysis: An application of solar radiation," *Waves Random Complex Media*, 2022. DOI: 10.1080/17455030.2022.2123571.

[28] M. Ramzan *et al.*, "A numerical study of the nanofluid flow over an exponentially stretching surface with Navier slip condition following Corcione model," *Int. J. Mod. Phys. B*, 2023. DOI: 10.1142/S0217979223502715.

[29] Y. M. Chu, S. Bashir, M. Ramzan, and M. Y. Malik, "Model-based comparative study of magnetohydrodynamics unsteady hybrid nanofluid flow between two infinite parallel plates with particle shape effects," *Math. Meth. Appl. Sci.*, vol. 46, no. 10, pp. 11568-11582, 2022. DOI: 10.1002/mma.8234.

[30] F. Shahzad *et al.*, "Thermal Amelioration in heat transfer rate using Oldroyd-B model hybrid nanofluid by CNTs-based kerosene oil flow in solar collector applications," *Waves Random Complex Media*, 2022. DOI: 10.1080/17555030.2022.2157511.

[31] W. Jamshed, M. R. Eid, F. Shahzad, R. Safdar, and MD. Shamshuddin, "Keller box analysis for thermal efficiency of magneto time-dependent nanofluid flowing in solar-powered tractor application applying nano-metal shaped factor," *Waves Random Complex Media*, 2022. DOI: 10.1080/17455030.2022.2146779.

[32] B. P. Geridonmez and H. Öztop, "MHD natural convection in a cavity in the presence of cross partial magnetic fields and Al_2O_3-water nanofluid," *Comput. Math. Appl.*, vol. 80, no. 12, pp. 2796–2810, 2020. DOI: 10.1016/j.camwa.2020.10.003.

[33] X. Zhang and Y. Zhang, "Experimental study on enhanced heat transfer and flow performance of magnetic nanofluids under alternating magnetic field," *Int. J. Therm. Sci.*, vol. 164, pp. 106897, 2021. DOI: 10.1016/j.ijthermalsci.2021.106897.

[34] X. Zhang and Y. Zhang, "Heat transfer and flow characteristics of Fe_3O_4-water nanofluids under magnetic excitation," *Int. J. Therm. Sci.*, vol. 163, pp. 106826, 2021. DOI: 10.1016/j.ijthermalsci.2020.106826.

[35] M. Ramzan *et al.*, "Thermophoretic particle deposition impact in the Oldroyd-B fluid flow influenced by a magnetic dipole with an exponential thermal heat source," *Int. J. Mod. Phys. B*, vol. 37, no. 06, pp. 2350059, 2023. DOI: 10.1142/S0217979223500595.

[36] B. J. Gireesha, M. Archana, B. Mahanthesh, and B. C. Prasannakumara, "Exploration of activation energy and binary chemical reaction effects on nano Casson fluid flow with thermal and exponential space-based heat source," *MMMS.*, vol. 15, no. 1, pp. 227–245, 2019. DOI: 10.1108/MMMS-03-2018-0051.

[37] W. Al-Kouz, K. Swain, B. Mahanthesh, and W. Jamshed, "Significance of exponential space-based heat source and inclined magnetic field on heat transfer of hybrid nanoliquid with homogeneous-heterogeneous chemical reaction," *Heat Transf.*, vol. 50, no. 4, pp. 4086–4102, 2021. DOI: 10.1002/htj.22065.

[38] K. Swain, M. Mishra, and P. K. Rout, "Magnetohydrodynamics flow of nanofluid past an elongating sheet with exponential space- based heat source and homogeneous-heterogeneous chemical reactions," *Int. J. Thermofluidic Sci. Technol.*, vol. 8, no. 3, pp. 080302, 2021. DOI: 10.36963/IJTST.2021080302.

[39] P. P. Humane, V. S. Patil, A. B. Patil, MD. Shamshuddin, and G. R. Rajput, "Dynamics of multiple slip boundaries effect on MHD Casson-Williamson double-diffusive nanofluid flow past an inclined magnetic stretching sheet," *Proc. Inst. Mech. E: J. Process Mech. Eng.*, vol. 236, no. 5, pp. 1906–1926, 2022. DOI: 10.1177/09544089221078153.

[40] M. A. A. Hamad, "Analytical solution of natural convection flow of a nanofluid over a linearly stretching sheet in the presence of magnetic field," *Int. Commun. Heat Mass Transf.*, vol. 38, no. 4, pp. 487–492, 2011. DOI: 10.1016/j.icheatmasstransfer.2010.12.042.

[41] MD. Shamshuddin and M. R. Eid, "n^{th} order reactive nanoliquid through convective elongated sheet under mixed convection flow with Joule heating effects," *J. Therm. Anal. Calorim.*, vol. 147, no. 5, pp. 3853–3867, 2022. DOI: 10.1007/s10973-021-10816-0.

[42] R. E. Bellman and R. E. Kalaba, *Quasilinearization and Nonlinear Boundary-Value Problems*. New York NY: Elsevier Publishing Company, 1965.

[43] S. S. Motsa, "A New spectral local linearization method for nonlinear boundary layer flow problems," *J. Appl. Math.*, vol. 2013, pp. 1–15, 2013. DOI: 10.1155/2013/423628.

[44] R. S. R. Gorla and I. Sidawi, "Free convection on a vertical stretching surface with suction and blowing," *Appl. Sci. Res.*, vol. 52, no. 3, pp. 247–257, 1994. DOI: 10.1007/BF00853952.

[45] W. A. Khan and I. Pop, "Boundary-layer flow of a nanofluid past a stretching sheet," *Int. J. Heat Mass Transf.*, vol. 53, no. 11–12, pp. 2477–2483, 2010. DOI: 10.1016/j.ijheatmasstransfer.2010.01.032.

[46] N. A. Shah *et al.*, "Significance of nanoparticle's radius, heat flux due to concentration gradient, and mass flux due to temperature gradient: The case of Water conveying copper nanoparticles," *Sci. Rep.*, vol. 11, no. 1, pp. 1–11, 2021. DOI: 10.1038/s41598-021-81417-y.

[47] K. K. Asogwa, M. D. Alsulami, B. C. Prasannakumara, and T. Muhammad, "Double diffusive convection and cross diffusion effects on Casson fluid over a Lorentz force driven Riga plate in a porous medium with heat sink: An analytical approach," *Int. Commun. Heat Mass Transf.*, vol. 131, pp. 105761, 2022. DOI: 10.1016/j.icheatmasstransfer.2021.105761.

[48] K. K. Asogwa, F. Mebarek-Oudina, and I. L. Animasaun, "Comparitive investigation of water-based Al_2O_3 nanoparticles through water-based CuO nanoparticles over an exponentially accelerated radiative Riga plate surface via heat transport," *Arab. J. Sci. Eng.*, vol. 47, no. 7, pp. 8721–8738, 2022. DOI: 10.1007/s13369-021-06355-3.